

Interannual Variability of Cold Air Outbreak in East Asia defined in Isentropic Coordinate

MUHAMMAD RAIS ABDILLAH, TOSHIKI IWASAKI, YUKI KANNO
GRADUATE SCHOOL OF SCIENCE, DEPARTMENT OF GEOPHYSICS, TOHOKU UNIVERSITY

1. Introduction

A recent study proposed a method to quantitatively measure cold air mass (CAM; Iwasaki et al. 2014; hereafter I14). It takes advantage of potential temperature surface which is convenient for tracking cold air. In mass-weighted isentropic zonal mean viewpoint, the center of extratropical direct circulation in northern hemisphere is located in 45°N and 850hPa (Iwasaki and Mochizuki 2012). This point is coincided with $\theta_T=280\text{K}$ level, which is suggested as an appropriate isentropic surface to measure CAM (I14). They found two major equatorward cold air outbreaks (CAO) in North Pole region. They are East Asian stream (EA stream) and North American stream (NA stream).

Shoji et al. (2014) performed a synoptic analysis related to EA stream defined in 90°-180°E longitude and 45°N latitude (hereafter EAS). They show the CAO formation and its impact. In addition, they found that western EA stream (EAS-W) and eastern EA stream (EAS-E) have different characteristics on their evolutions. In this study, we raise a topic of EA stream interannual variability which has not been discussed previously. We focus on the difference between EAS-W and EAS-E.

2. Data and definition of cold air outbreak

We use Japanese 55-year Reanalysis (JRA-55) dataset (Kobayashi et al. 2015). The monthly precipitation data is the Precipitation Reconstruction (PREC). We also use the Sea Surface Temperature (SST) data from HadISST1 dataset. In this study, we average the data in Dec-Jan-Feb (DJF) to obtain the winter mean. The analysis period covers 56 boreal winters from 1958 to 2013. Here, the winter of 1958 refers to the DJF 1958/59. The statistical significance levels used in this study are calculated based on a two-sided Student's t test. In addition, we use daily interpolated-Outgoing Long-wave Radiation (OLR) data from CPC/NOAA for lagged-day analysis, which the period is winter 1979 to winter 2012.

The definition of CAO in East Asia is similar to the index proposed by Shoji et al. (2014) (hereafter S14). The equations of polar CAM amount (DP), CAM flux (\mathbf{F}), and associated diabatic change rate [$G(\theta_T)$] below potential temperature θ_T are presented in I14. Our analysis emphasizes the variability of meridional component of the CAM flux, particularly related to equatorward flow of CAM (F_{-v}). In East Asia, the maximum CAO are observed at 45°N between 90°E and 180°E, hence this region is considered as the exit pathway (S14). In short, the CAO index in East Asia (EAS) was defined as

$$EAS \equiv \frac{a \cos \phi}{g} \int_{90E}^{180E} F_{-v} d\lambda \Big|_{\phi=45N}, \quad (1)$$

where F_{-v} , ϕ , λ , a , and g denote: southward component of CAM flux below $\theta_T=280\text{K}$, latitude, longitude, earth radius, and gravity acceleration, respectively. Then, the EAS-W and the EAS-E index was simply defined as below:

$$EAS-W \equiv \frac{a \cos \phi}{g} \int_{90E}^{135E} F_{-v} d\lambda \Big|_{\phi=45N}, \quad (2)$$

$$EAS-E \equiv \frac{a \cos \phi}{g} \int_{135E}^{180E} F_{-v} d\lambda \Big|_{\phi=45N}. \quad (3)$$

For regression and correlation analysis, the indices are normalized by each standard deviation and the climatological means of atmospheric dataset are removed.

3. Interannual variation of EA stream

Figure 1a shows the climatology of CAM flux and the location of EAS, EAS-W and EAS-E. Interannual variations of these indices are presented in Fig. 1b. The intensity of EAS is obviously far higher than EAS-W or EAS-E. The EAS-E has larger interannual standard deviation compared to EAS-W (Fig. 1b). Several strong EAS-W winters appear in 2011, 1967, 1985, and 1976 winter, sorted from the smallest to the largest value. Remarkably, the winter of 1976 also appears as the strongest EAS-E, followed by 1963, 2002, and 1997 winter.

Moreover, the EAS-W and EAS-E show distinct decadal variations (Fig. 1b). The EAS-W shows a robust weakening after mid-1980s which is possibly similar to the decadal weakening of East Asian winter monsoon (EAWM) (Wang and Chen 2014; hereafter WC14). During this period, the noteworthy features is the significant decrease of cold wave frequency (Wang et al. 2009). The EAS-W may be closely linked to Siberian high (SH) variability (Gong et al. 2001, hereafter GO01). On the other hand, the EAS-E begins a weakening pattern and then steadily increasing to early-2000s. Generally, the EAS-E are somewhat similar to the variation of Aleutian low (AL) index (Overland et al. 1999, hereafter OV99).

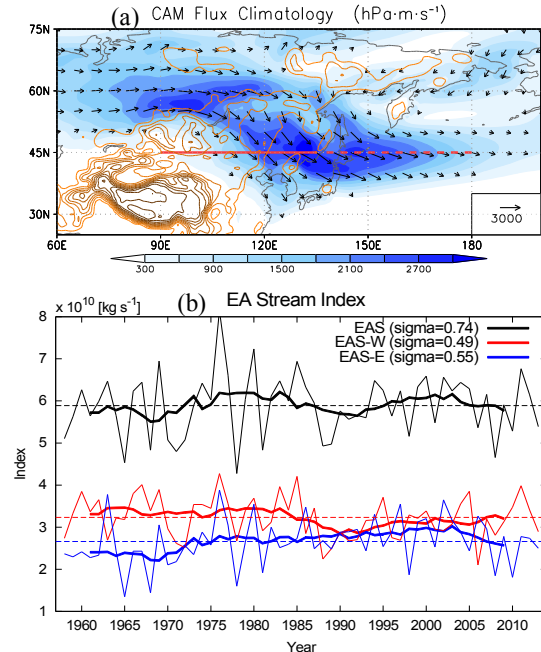


Figure 1 (a) Climatology of cold air mass flux (vector) and its magnitude (shaded) for the DJF 1958-2013 (unit: hPa m s^{-1}). Thick and dashed red lines show the location of EAS-W and EAS-E, respectively. Brown lines represent topography with 500 m interval. (b) Time-series of EA stream indices (unit: $10^{10} \text{ kg s}^{-1}$). Thin lines represent annual variation while thick lines represent decadal components expressed by a 9-year running mean. Dashed lines denote the mean values. Sigma notation in the legend represents interannual standard deviation

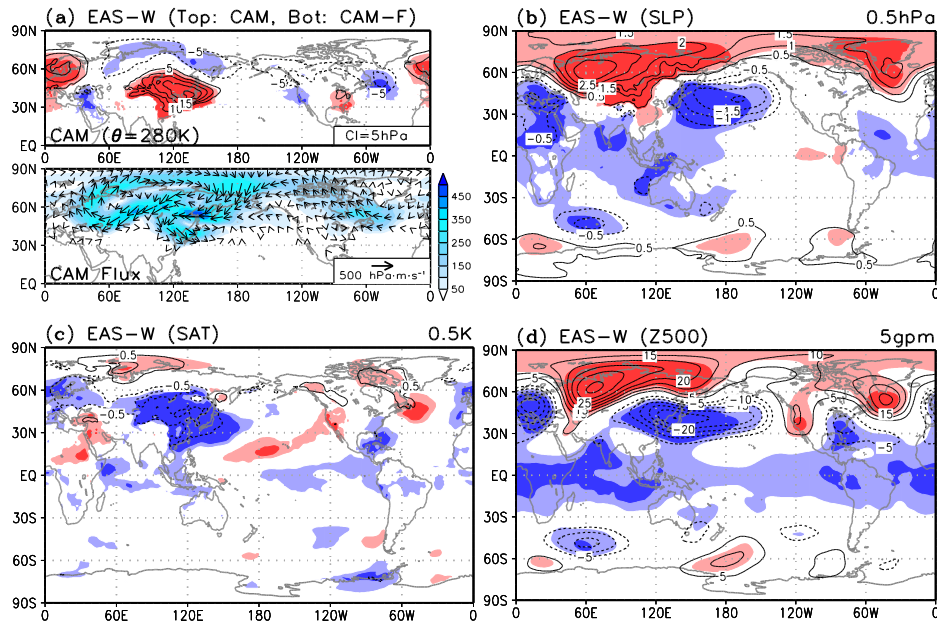


Figure 2 Selected climate variables regressed with EAS-W index (90°-135°E). Contour lines and vectors represent regression coefficients. (a) Top: cold air mass, bottom: CAM flux (vector) and its intensity (shaded). (b) Sea level pressure. (c) Surface temperature at 2 m. (d) 500hPa geopotential height. Contour intervals and units are shown in top-right of each panel. Light (dark) shading indicate 90% (99%) statistical significance (except in (a) bottom)

4. Climate anomalies associated with EA stream index

(a) Western EA stream (EAS-W)

Figure 2 exhibits several climate anomalies which are associated with EAS-W index. The exerted cold air is evident in East Asia (Fig. 2a upper). This is highly influenced by pressure contrast over Eurasian continent (i.e., SH) and the adjacent oceans (Fig. 2b). The significant negative SLP is observed in the southwestern AL which is highlighted by WC14 as a key region on the EAWM. Correlation coefficient (CC) of EAS-W and SH/AL index is 0.79/-0.35 (Table 1). Fig. 2c and 2d show significant impacts on cooling in East Asia and deepened East Asian trough, respectively. The CC of EAS-W index and East Asian surface air temperature (EA-SAT) is -0.60. Overall, the EAS-W signatures are closely similar to the EAWM pattern. The robust correlation between EAS-W index and EAWM index is 0.85. On the other hand, the EAS-W is significantly correlated with Arctic Oscillation (AO; Thompson and Wallace 1998, hereafter TW98) as shown in Table 1 ($r = -0.47$). The negative AO tends to amplify SH. Long lasting cold surges have been reported to be dominant during negative AO. Therefore, AO may influence the EAS-W outbreak.

Despite an enormous excess of CAM, the reduction signal in northern Eurasia is relatively small (Fig. 2a upper). It is possibly due to large intraseasonal variability of the CAO formation which can be induced by both wave-train (Atlantic origin) type and north Pacific blocking type (Takaya and Nakamura 2005). In northern mid-troposphere, we notice a wave-train pattern (Fig. 2d), which may resemble Eurasian (EU) teleconnection pattern (Wallace and Gutzler 1981, hereafter WG81). Moreover, a north-south seesaw pattern in northeast Asia quite corresponds to negative phase of western Pacific (WP) pattern (WG81). CC between EAS-W index with EU and WP index are exceeding 99% statistical significance (0.75 and -0.48; Table 1).

In tropical region, negative height anomaly zonally elongates in tropics (Fig. 2d). Significant cold SST over central-eastern Pacific also appears (Fig. 4a). Figure 4b shows a distinct enhanced Walker circulation which is associated with wet (dry) area over Maritime continent and west Pacific (central Pacific and Indian Ocean). These patterns resemble a typical La Nina-like pattern. Therefore, La Nina events tend to enhance CAO in EAS-W. CC between EAS-W and Nino-3 index is -0.28 during 56 winters (Table 1), exceeding 95% significance level.

(b) Eastern EA stream (EAS-E)

On the other hand, the surplus cold air maintained by EAS-E index concentrates over western North Pacific Ocean (Fig. 3a upper). The abundant reduction of cold air mass is observed in northeast America. It seems that the EAS-E is highly connected to the North Pacific variability (i.e., AL) than SH. As shown in Fig. 3b, the AL is strongly enhanced, while considerable high SLP exists in the eastern Siberia. The CC of EAS-E and AL/SH index is -0.76/0.03 (Table 1). Therefore, significant cooling is observed over East Asian ocean instead over the land (Fig. 3c). In mid-troposphere, the Pacific/North American (PNA) pattern (WG81) is evident (Fig. 3d). Although

Table 1. Correlation coefficients between EA stream indices and several climate indices. Superscript (*) and (**) indicate the index exceeding 99% and 99.99% statistical significance, respectively

Index	EAS-W	EAS-E	EAS	Reference
EA-SAT	-0.60**	-0.07	-0.45*	SAT (20°-35°N, 105°-130°E)
SH	0.79**	0.03	0.55**	GO01
AL	-0.35*	-0.75**	-0.80**	OV99
EAWM	0.85**	0.07	0.62**	WC14
EU	0.75**	0.04	0.53*	WG81
WP	-0.48*	0.01	-0.31	WG81
AO	-0.47*	0.08	-0.25	TW98
PNA	0.28	0.77**	0.76**	WG81
Nino-3	-0.28	0.35*	0.08	SST (5°S-5°N, 150°-90°W)

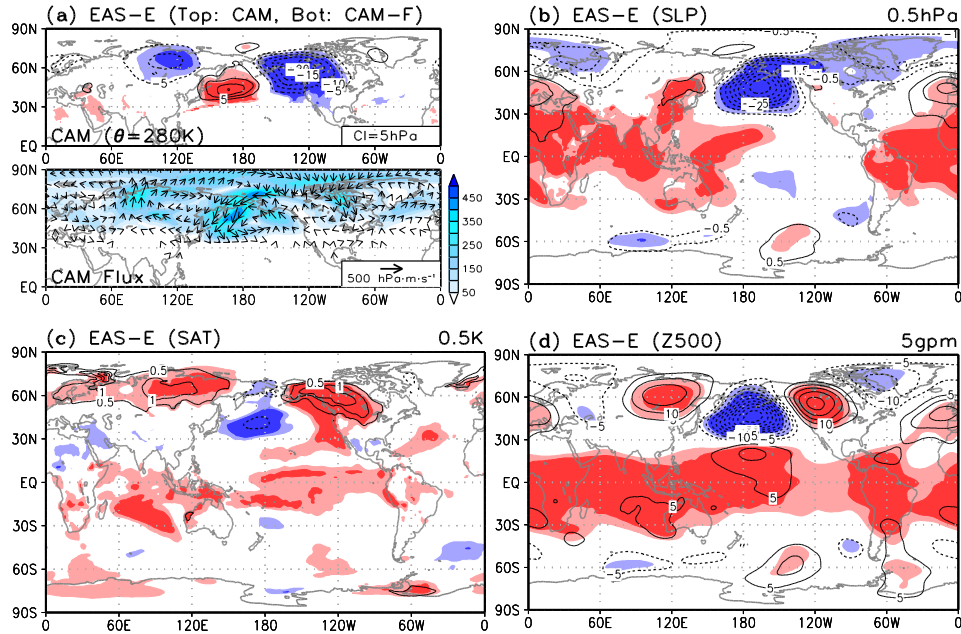


Figure 3 As in Fig. 2 but for EAS-E index (135°-180°E)

a negative height anomaly in downstream PNA pattern (i.e., southeast U.S.) is not seen, the correlation of PNA index with EAS-E index is quite high (0.77).

In tropical region, we observe the zonally elongated positive height anomalies (Fig. 3d), which can be attributed to the warm pools SST in Indo-Pacific regions (Fig. 4c). The reversed Walker-circulation is evident in EAS-E pattern (Fig 4d). The maritime continent shows suppressed precipitation and the central Pacific shows enhanced precipitation. The CC between EAS-E index and Nino-3 index is 0.35 (Table 1), greater than 99% significance level. Contrary with the EAS-W, El Niño tends to enhance CAO in the EAS-E region.

(c) Entire EA stream (EAS)

The EAS index shows significant climate signatures in mid- or high-latitudes (not shown). The excess of cold air mass widely elongates from inland Asia to central North Pacific but

with less intensity compared to EAS-W or EAS-E. The CC of the EAS index and the mentioned climate indices are shown in Table 1. The interesting feature of EAS is the suppression of tropical connection. We do not detect any significant regression of SST or precipitation with EAS in tropics. As discussed before, the ENSO gives seesaw relationship to EAS; hence the signal becomes diminished when the EAS index is calculated.

5. Distinguishing the signatures over tropical region into precursor and impact

In this section, we investigate the evolution of tropical precipitation associated with EA stream. As shown in Fig. 4b and 4d, the EAS-W and EAS-E exhibit significant anomalous convection over Maritime Continent (MC), Central Pacific (CP), and Indian Ocean (IO). We are curious about when the pattern is prominent, does it appear during preceding CAO or after CAO? (Hereafter, the CAO event is set on Day 0). Therefore,

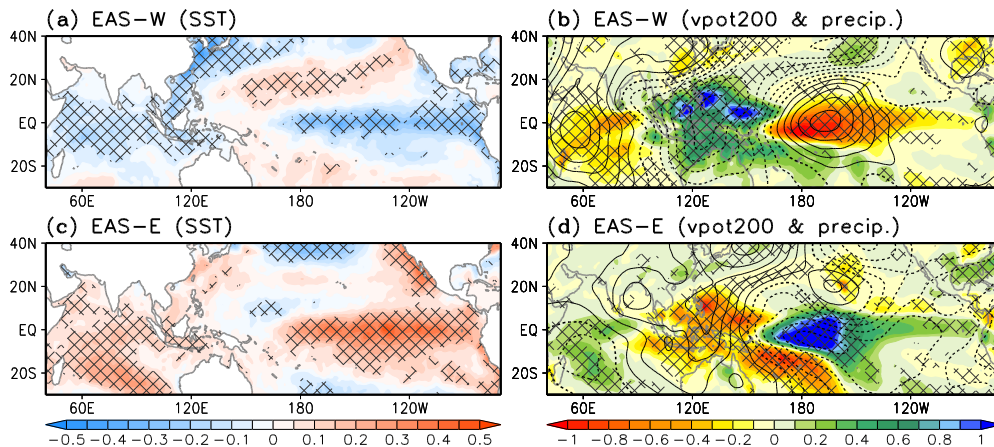


Figure 4 (left) SST (shaded) regressed with EAS-W (a) and EAS-E index (c). (right) Precipitation rate (shaded) and velocity potential at 200hPa (vpot200; contour) regressed with EAS-W (b) and EAS-E index (d). Interval for SST, precipitation, and vpot200 are 0.05°C, 0.1mm/day, and 1.5×10⁵m²/s, respectively. Hatched areas in (left) and (right) exceed 90% statistical significance level of SST and precipitation, respectively

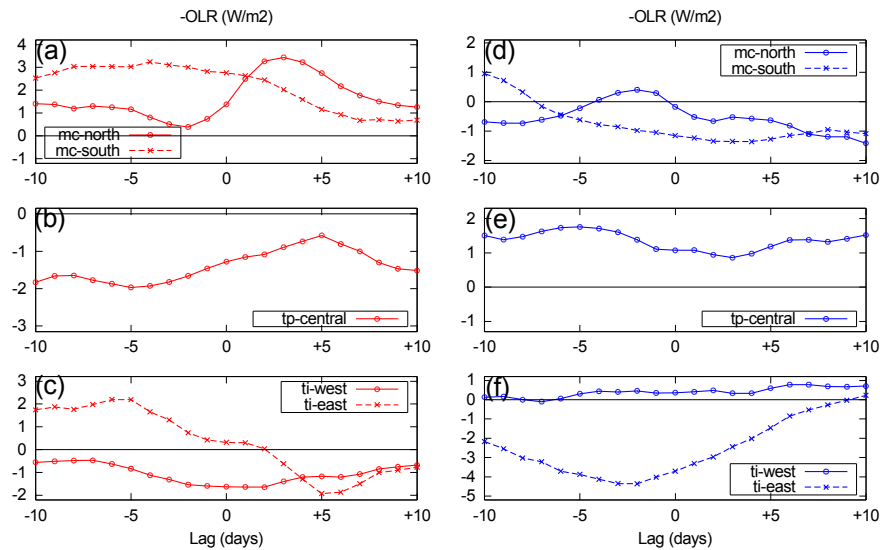


Figure 5 Lag-day regression of EAS-W index (left panel, red lines) and EAS-E index (right panel, blue lines) with several daily OLR anomaly indices around tropical region. OLR data is multiplied by -1. Top panel represents convective response for northern Maritime Continent (5°-20°N; 100°-140°E) and southern Maritime Continent (20°-5°S; 105°-150°E). Middle panel, same as top but for central Pacific Ocean (10°S-10°N; 160°E-150°W). For bottom panel, same as top but for western (5°S-10°N; 40°-70°E) and eastern Indian Ocean (5°S-5°N; 80°-100°E)

we perform lagged-day regression analysis of EAS-W/EAS-E index with anomalous OLR data in region of interest: northern MC (5°-20°N; 100°-140°E), southern MC (20°-5°S; 105°-150°E), CP (10°S-10°N; 160°E-150°W), western IO (5°S-10°N; 40°-70°E), and eastern IO (5°S-5°N; 80°-100°E). Before calculation, the OLR data is multiplied by -1.

In EAS-W pattern, the OLR anomalies in MC show enhanced convection at before and after the CAO event (Fig. 5a), indicating the strengthening local Hadley circulation. The substantial feature appears around Day +3 in northern MC. This exhibits enhanced convection as the impact of CAO. On the other hand, southern MC shows relatively strong convection before the event and the impact is less seen after the event. Hence, the southern MC is observed as a precursor of CAO. In CP region (Fig. 5b), the suppressed convection is dominant before the outbreak which may be associated with enhanced Walker circulation. It is regarded as the precursor. In western IO (Fig. 5c), the signal is small. However, the eastern IO shows enhanced convection before the CAO and rapid decreasing after the CAO.

In EAS-E pattern, the amplitude and the oscillation are quite small in MC (Fig. 5d). For northern and southern MC, the suppressed convection is distinctly seen following the CAO event. The enhanced convection over CP seems to be dominant at entire days (Fig. 5e). The noteworthy pattern is shown in Fig. 5f. Before the event, the convection over eastern IO is deeply suppressed then gradually weaker.

As in S14 analysis, the impact of the EAS-E on tropical region is not observed in surface wind field analysis. It is expected that we could not observe some convections excited by low-level CAO in EAS-E. However, some anomalies or teleconnections between EAS-E and tropical convection exist in preceding or after the surge. In EAS-W, the downward Walker circulation and southern MC seem to be precursors. The physical mechanisms are still not clear. Further studies are needed to investigate these patterns.

6. Conclusion

The EAS-W pattern exhibits excess cold air mass and negative surface air temperature (SAT) from East Asia to low-latitude region. The deepened East Asian trough and positive SLP anomalies over Eurasian continent are evident. The EAS-W signatures are closely related to Siberian high (SH) variability. The enhanced convection over Maritime continent (MC) is evident, and the northern part of MC is attributed as the impact of CAO event in EAS-W. The tropical SST resembles La Nina-like pattern, thus implying cool ENSO tends to induce EAS-W.

On the contrary, the EAS-E signal is less significant in East Asia: the negative SAT over land does not appear and the CAO does not propagate to low-latitude. The Aleutian low (AL) plays a major role in EAS-E. Tropical signatures described by EAS-E are reversely depicted compared to EAS-W pattern. The El Nino-like patterns appear significantly in the SST and precipitation map. Therefore, the warm phase of ENSO tends to induce EAS-E.

Reference

- Gong, D.-Y., S.-W. Wang, and J.-H. Zhu, 2001: *Geophys. Res. Lett.*, **28**, 2073–2076, doi:10.1029/2000GL012311.
- Iwasaki, T., and Y. Mochizuki, 2012: *Sola*, **8**, 115–118, doi:10.2151/sola.2012-029.
- , T. Shoji, Y. Kanno, M. Sawada, M. Ujije, K. Takaya, and M. Ujje, 2014: *J. Atmos. Sci.*, **71**, 2230–2243, doi:10.1175/JAS-D-13-058.1.
- Kobayashi, S., and Coauthors, 2015: *J. Meteorol. Soc. Japan*, doi:10.2151/jmsj.2015-001.
- Overland, J. E., J. M. Adams, and N. A. Bond, 1999: *J. Clim.*, **12**, 1542–1548, doi:10.1175/1520-0442(1999)012<1542:DVOTAL>2.0.CO;2.
- Shoji, T., Y. Kanno, T. Iwasaki, and K. Takaya, 2014: *J. Clim.*, **27**, 9337–9348, doi:10.1175/JCLI-D-14-00307.1.
- Takaya, K., and H. Nakamura, 2005: *J. Atmos. Sci.*, **62**, 4423–4440, doi:10.1175/JAS3629.1.
- Thompson, D. W. J., and J. M. Wallace, 1998: *Geophys. Res. Lett.*, **25**, 1297–1300, doi:10.1029/98GL00950.
- Wallace, J. M., and D. S. Gutzler, 1981: *Mon. Weather Rev.*, **109**, 784–812, doi:10.1175/1520-0493(1981)109<0784:TITGHF>2.0.CO;2.
- Wang, L., and W. Chen, 2014: *J. Clim.*, **27**, 2361–2374, doi:10.1175/JCLI-D-13-00086.1.
- , R. Huang, L. Gu, W. Chen, and L. Kang, 2009: *J. Clim.*, **22**, 4860–4872, doi:10.1175/2009JCLI2973.1.